Ultra-thin single-layer transparent geometrical phase gradient metasurface and its application to high-gain circularly-polarized lens antenna*

Tang-Jing Li(李唐景)†, Jian-Gang Liang(梁建刚), Hai-Peng Li(李海鹏), and Ya-Qiao Liu(刘亚峤)

Air and Missile Defense College, Air Force Engineering University, Xi'an 710051, *China*

(Received 3 March 2016; revised manuscript received 6 May 2016; published online 20 July 2016)

A new method to design an ultra-thin high-gain circularly-polarized antenna system with high efficiency is proposed based on the geometrical phase gradient metasurface (GPGM). With an accuracy control of the transmission phase and also the high transmission amplitude, the GPGM is capable of manipulating an electromagnetic wave arbitrarily. A focusing transmission lens working at Ku band is well optimized with the F/D of 0.32. A good focusing effect is demonstrated clearly by theoretical calculation and electromagnetic simulation. For further application, an ultra-thin single-layer transmissive lens antenna based on the proposed focusing metasurface operating at 13 GHz is implemented and launched by an original patch antenna from the perspective of high integration, simple structure, and low cost. Numerical and experimental results coincide well, indicating the advantages of the antenna system, such as a high gain of 17.6 dB, the axis ratio better than 2 dB, a high aperture efficiency of 41%, and also a simple fabrication process based on the convenient print circuit board technology. The good performance of the proposed antenna indicates promising applications in portable communication systems.

Keywords: geometrical phase gradient metasurface, circular polarization, lens antenna

PACS: 41.20.Jb, 29.27.Hj, 84.40.Ba **DOI:** 10.1088/1674-1056/25/9/094101

1. Introduction

In recent years, phase gradient metasurfaces (PGMs), proposed by Yu *et al.*,[1] have induced a great impetus and been applied widely. Completely distinct from the phase accumulation in conventional metamaterials,[2] the PGM presents a strong control over the phase by suitably tailoring phase discontinuities on the dielectric surface, providing a promising route to construct ultra-thin planar devices. With the unprecedented control of electromagnetic (EM) wavefronts, PGMs have found wide applications in cloaks,[3,4] focusing lenses,[5–7] holography,[8,9] polarization beam splitter,[10,11] beam scanning,[12,13] polarization keeping,[14] polarization conversion,[15] to name a few. However, the relatively low transmission efficiency for the transmissive metasurface has limited its further applications. Multilayer transmissive PGMs improve the transmission efficiency significantly.[16,17] However, the multilayer technology brings a great challenge for the fabrication and a high cost. Geometrical phase gradient metasurface (GPGM), with full control of transmission phase and high transmission amplitude, provides a good way to solve all issues aforementioned.

Circularly polarized (CP) antennas have been applied to numerous wireless communication systems for their attractive features, such as light weight, low cost, ease of fabrication, especially the stable date transmission rate without reference to the polarization orientation between the transmitter and the receiver.[18] However, conventional CP antennas suffer from low radiation gain, large cross polarization, and complex feeding system. Moreover, the CP antenna based on GPGM has been reported rarely. The insufficient technology makes the attempt of employing GPGM in high gain CP antenna design a challenging and pressing task.

In this paper, a single-layer transmissive GPGM is proposed for the first time. The phase gradient on the metasurface is obtained by rotating the designed element. The transmission coefficient T_x for x polarization and T_y for y polarization reach about 0.9 for the element, and the transmission phase difference between them keeps π. Both aspects play an essential role in polarization and phase control. The rest of the paper is arranged as follows. Section 2 shows the element structure, the characterization of the unit cell and also the working principle of GPGM. Furthermore, the focusing lens based on the GPGM is calculated, EM simulated and further analyzed. Section 3 discusses the simulated and measured performances of the high-gain antenna based on the focusing lens. Finally, the paper is summarized.

2. Transmissive GPGM design

2.1. Unit cell design

We utilize the spin element to compensate the phase deviation of a circularly polarized wave. Figure 1 shows the illustration of the element rotation method. Suppose a right-hand

*Project supported by the National Natural Science Foundation of China (Grant No. 61372034).

†Corresponding author. E-mail: litangjing666@sina.com

© 2016 Chinese Physical Society and IOP Publishing Ltd

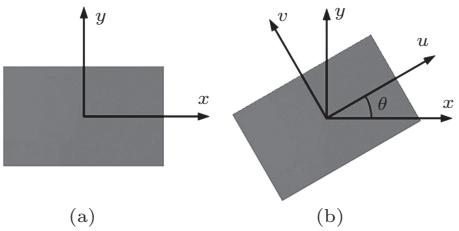


Fig. 1. Diagram of spin element in (a) *xyz* coordinates and (b) rotated coordinates.

circularly polarized (RCP) wave transmitted onto the unit cell along the z direction as shown in Fig. 1(a). The E field of the transmitted RCP wave is

$$\boldsymbol{E}_{\rm i} = E_0(\boldsymbol{x} - {\rm j}\boldsymbol{y})\,{\rm e}^{-{\rm j}kz}, \tag{1}$$

and the transmissive wave can be calculated as

$$\boldsymbol{E}_{\rm t} = E_0(\boldsymbol{x}T_x\,{\rm e}^{{\rm j}\phi_x} - {\rm j}\boldsymbol{y}T_y\,{\rm e}^{{\rm j}\phi_y})\,{\rm e}^{-{\rm j}kz}, \tag{2}$$

where E_0 is the amplitude of the transmitted wave, T_x and T_y are the transmissive coefficient amplitudes of the x-polarized and y-polarized wave components, ϕ_x and ϕ_y are the phase shifts of the x-polarized and y-polarized components of the incident wave. When the metallic structure is rotated by θ as shown in Fig. 1(b), the rotated coordinate can be written as

$$\begin{cases} \boldsymbol{x} = \boldsymbol{u}\cos\theta - \boldsymbol{v}\sin\theta, \\ \boldsymbol{y} = \boldsymbol{u}\sin\theta + \boldsymbol{v}\cos\theta, \end{cases} \tag{3}$$

and the incident wave in the rotated coordinate is expressed as

$$\begin{aligned} \boldsymbol{E}_{\rm i} &= E_0[(\boldsymbol{u}\cos\theta - \boldsymbol{v}\sin\theta) - {\rm j}(\boldsymbol{u}\sin\theta + \boldsymbol{v}\cos\theta)]\,{\rm e}^{-{\rm j}kz} \\ &= E_0(\boldsymbol{u} - {\rm j}\boldsymbol{v})\,{\rm e}^{-{\rm j}kz}\,{\rm e}^{-{\rm j}\theta}. \end{aligned} \tag{4}$$

Then, the transmissive wave can be calculated by

$$\boldsymbol{E}_{\rm t} = E_0(\boldsymbol{u}T_u\,{\rm e}^{{\rm j}\phi_u} - {\rm j}\boldsymbol{v}T_v\,{\rm e}^{{\rm j}\phi_v})\,{\rm e}^{-{\rm j}kz}\,{\rm e}^{-{\rm j}\theta}. \tag{5}$$

As $\phi_x = \phi_u$ and $\phi_y = \phi_v$, $T_x = T_u$ and $T_y = T_v$, in xyz coordinate, the transmissive wave can be written as

$$\begin{aligned} \boldsymbol{E}_{\rm t} &= E_0[(\boldsymbol{x}\cos\theta + \boldsymbol{y}\sin\theta)T_x\,{\rm e}^{{\rm j}\phi_x} \\ &\quad - {\rm j}(-\boldsymbol{x}\sin\theta + \boldsymbol{y}\cos\theta)T_y\,{\rm e}^{{\rm j}\phi_y}]\,{\rm e}^{-{\rm j}kz}\,{\rm e}^{-{\rm j}\theta} \\ &= \frac{E_0}{2}[(\boldsymbol{x} + {\rm j}\boldsymbol{y})(T_x\,{\rm e}^{{\rm j}\phi_x} - T_y\,{\rm e}^{{\rm j}\phi_y})\,{\rm e}^{-{\rm j}2\theta} \\ &\quad + (\boldsymbol{x} - {\rm j}\boldsymbol{y})(T_x\,{\rm e}^{{\rm j}\phi_x} + T_y\,{\rm e}^{{\rm j}\phi_y})]\,{\rm e}^{-{\rm j}kz}. \end{aligned} \tag{6}$$

It should be highlighted that the transmissive wave contains two parts

$$\boldsymbol{E}_{\rm t(LCP)} = \frac{E_0}{2}(\boldsymbol{x} + {\rm j}\boldsymbol{y})(T_x\,{\rm e}^{{\rm j}\phi_x} - T_y\,{\rm e}^{{\rm j}\phi_y})\,{\rm e}^{-{\rm j}kz}\,{\rm e}^{-{\rm j}2\theta}, \tag{7}$$

$$\boldsymbol{E}_{\rm t(RCP)} = \frac{E_0}{2}(\boldsymbol{x} - {\rm j}\boldsymbol{y})(T_x\,{\rm e}^{{\rm j}\phi_x} + T_y\,{\rm e}^{{\rm j}\phi_y})\,{\rm e}^{-{\rm j}kz}, \tag{8}$$

where $\boldsymbol{E}_{\rm t(RCP)}$ and $\boldsymbol{E}_{\rm t(LCP)}$ are the right-hand rotation and left-hand rotation components of the transmissive wave, respectively. When $T_x = T_y = T$ and $|\phi_x - \phi_y| = \pi$, equations (7) and (8) can be written as

$$\begin{aligned} \boldsymbol{E}_{\rm t(LCP)} &= \frac{TE_0}{2}(\boldsymbol{x} + {\rm j}\boldsymbol{y})(1 - {\rm e}^{{\rm j}(\pm\pi)})\,{\rm e}^{{\rm j}\phi_x}\,{\rm e}^{-{\rm j}kz}\,{\rm e}^{-{\rm j}2\theta} \\ &= T(\boldsymbol{x} + j\boldsymbol{y})\,{\rm e}^{{\rm j}\phi_x}\,{\rm e}^{-{\rm j}kz}\,{\rm e}^{-{\rm j}2\theta}, \end{aligned} \tag{9}$$

$$\begin{aligned} \boldsymbol{E}_{\rm t(RCP)} &= \frac{TE_0}{2}(\boldsymbol{x} - {\rm j}\boldsymbol{y})(1 + {\rm e}^{{\rm j}(\pm\pi)})\,{\rm e}^{{\rm j}\phi_x}\,{\rm e}^{-{\rm j}kz} \\ &= 0. \end{aligned} \tag{10}$$

It is obvious that the transmissive wave only has left-hand rotation component which is opposite to the incident wave and the shift of transmissive wave phase is equal to twice the angle of rotation (θ), and the condition is the same as the left-hand circularly polarized (LCP) transmitted wave. Here, the working principle of the element can be obtained clearly. For one thing, $|\phi_x - \phi_y| = \pi$ is necessary to ensure a pure RCP or LCP. For another, T_x and T_y should be equal and as close as 1 to improve the transmissive efficiency.

According to the design principle, the structure of a well-optimized cell is shown in Fig. 2. The unit cell is composed of two metallic layers and one intermediate dielectric layer. The metal structure is built by a circle ring with a modified H-shaped wire embedded in. More importantly, the designed element will have an anisotropic phase response for orthogonally polarized waves thanks to its asymmetric structure. Specifically, there is a resonance around 13 GHz for y-polarized incidence, while no resonance exists for x polarization, which yields different transmission phases. The geometrical parameters of the unit cell are set as $r = 3.3$ mm, $a = 2.1$ mm, $b = 1.8$ mm, $c = 1.4$ mm, $k = 0.2$ mm, and $p = 7$ mm. The thickness h and the dielectric constant of the substrate are 1.5 mm and 2.65, respectively. It is necessary to emphasize that the electric size of the element is only $0.3\lambda_0$ at the center frequency of 13 GHz. With the great improvements in efficiency and size reduction, the metasurface sample constituted by this element will have accurate phase control for transmissive beams.

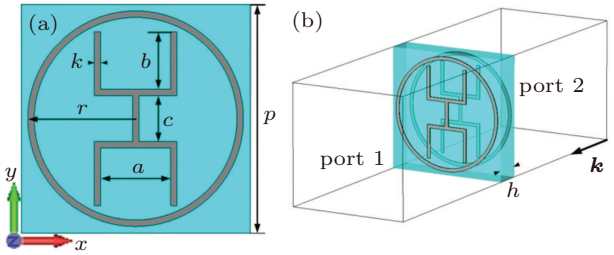


Fig. 2. (color online) Structure of the GPGM element and the simulated setup. (a) Top view and (b) perspective view.

Figure 3 plots the phase and amplitude of the transmissive wave under x-polarized and y-polarized wave illumina-

tion. It is exciting to mention that and $T_x = T_y$ are observed at 13 GHz, which is essential to ensure a pure CP wave. Meanwhile, the amplitudes of the x-polarized and y-polarized transmissive waves have both reached as high as 0.9, indicating high transmission efficiency.

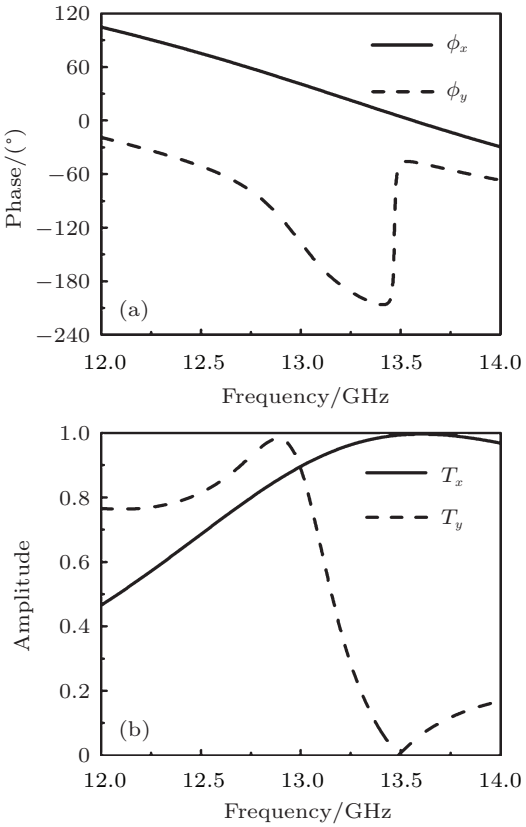


Fig. 3. (a) Phase and (b) amplitude of transmissive wave under x-polarized and y-polarized plane wave illumination.

To demonstrate the characterization of the geometrical phase, the transmitted RCP plane wave along the z direction is used to illuminate the optimized unit cell with the simulation setup shown in Fig. 2(b). The element is rotated with a step of 30°, and then the phase and amplitude of transmissive wave (LCP) are shown in Fig. 4. As expected, the proposed element achieves an accurate phase shift of 2θ. Moreover, the

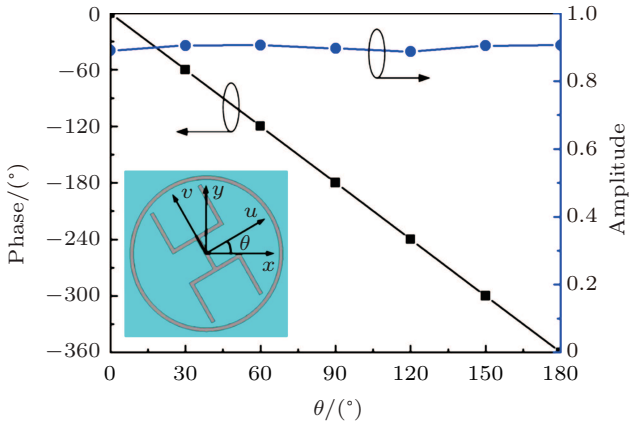


Fig. 4. (color online) The phase and amplitude of transmissive wave under RCP plane wave illumination at 13 GHz.

transmission amplitudes keep constant at about 0.9. The perfect phase as well as the high cross-polarization transmission efficiency make the element a good candidate for transmission system, which plays an important role in communication system and radar engineering.

2.2. Focusing GPGM design

The demonstration of geometrical phase indicates that the proposed transparent element is promising to achieve anomalous phenomenon, such as focusing, deflection, and hologram. More importantly, these applications are capable of high efficiency based on the high transmission coefficient of the element. Here, in order to demonstrate the good performance of the element, a focusing lens is designed. To achieve the planar focusing lens, the refracted phase should satisfy the parabolic profile. The required transmission phase profile on the GPGM is calculated by

$$\varphi(x,y) = \frac{2\pi}{\lambda_0}(\sqrt{x^2+y^2+f^2} - f) + \varphi_0, \tag{11}$$

where f is the focal distance, λ_0 is the wavelength in free space and φ_0 is the reference phase. In this work, an RCP focusing lens is designed for example. It is worth noting that the focusing point can be chosen arbitrarily, where $f = \lambda = 23$ mm is selected for the purpose of generality. To verify the focusing effect, we use 11×11 unit cells to satisfy the parabolic profile in the xoy plane according to Eq. (11). The calculated phase distribution is shown in Fig. 5(a), and figure 5(b) depicts the topology of designed lens. The GPGM is illuminated with the RCP plane wave propagating along the z direction. Figure 6 shows the power-flow distributions in the xoz plane and yoz plane at 13 GHz. It is obvious that almost all the power passes through the lens and the transmissive waves focus at the designed focusing point, which can be demonstrated according to Fig. 6(c). For further analysis, the reflected power is very weak, as observed from the power distributions. The good performance of RCP lens is promising in high-gain antenna systems.

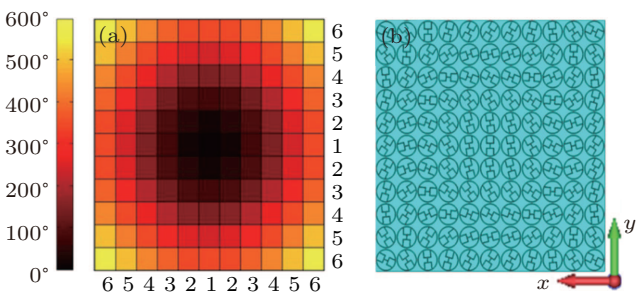


Fig. 5. (color online) (a) Corresponding phase distribution and (b) GPGM.

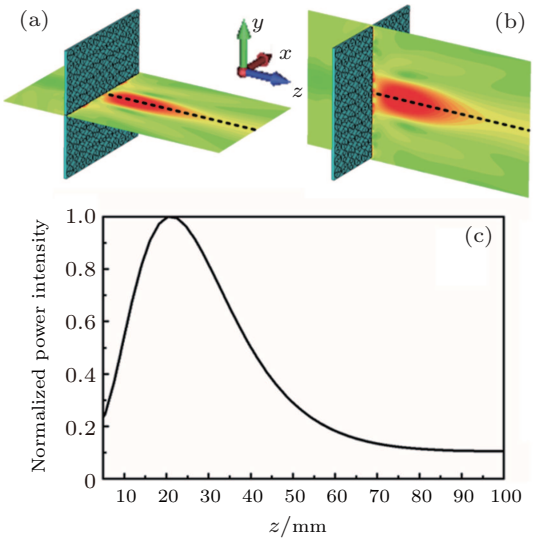


Fig. 6. (color online) The power flow in (a) the *xoz* plane and (b) *yoz* plane. (c) The normalized power intensity on the *z* axis under RCP plane wave at 13 GHz.

3. Lens antenna design

In the above section, we have verified that the designed focusing lens is capable of focusing a circularly polarized plane wave. According to the reversibility principle of EM wave propagation, a spherical-like wave that radiates from the point source on a focal point can be transformed into a plane wave by the lens. Then we put an RCP patch antenna with a peak gain of 6.4 dB working at 13 GHz as reference. We can observe the distribution of electric field in near field without and with the GPGM in Fig. 7. It is obvious that the GPGM lens transforms spherical-like waves into high directivity plane waves, as expected.

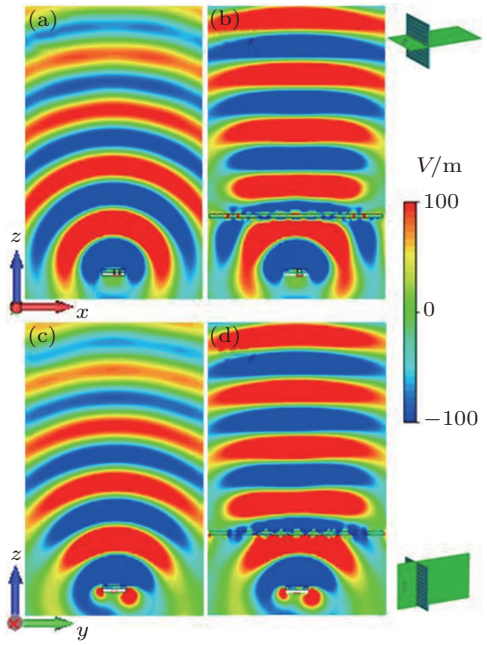


Fig. 7. (color online) Simulated electric field distribution at 13 GHz in (a), (b) the *xoz* plane and (c), (d) *yoz* plane, respectively, for the patch antenna (a), (c) without and (b), (d) with the GPGM.

Since the patch antenna is an unideal point source, the phase center is not strictly located at 23 mm, and should be optimized to achieve a good performance. Here, the length is well designed at 25 mm. Figure 8 shows the 3D simulated far-field radiation pattern at 13 GHz. It can be seen clearly that the gain reaches 17.6 dB at the center frequency. A further analysis indicates that an enhancement of 11.2 dB is achieved compared with that of the bare patch antenna.

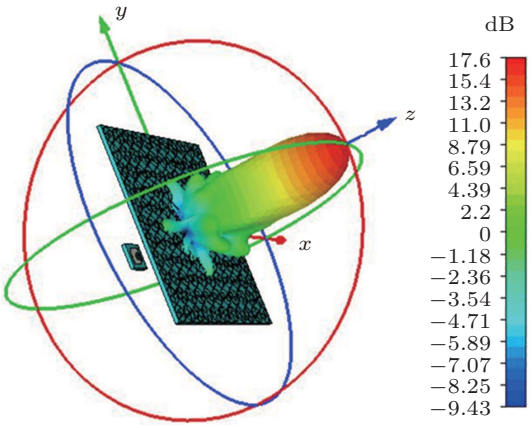


Fig. 8. (color online) 3D simulated far-field radiation pattern at 13 GHz.

In order to verify the simulation, the GPGM lens and patch antenna are fabricated with the photograph shown in Fig. 9. The measurement is carried out on the antenna test system in a microwave anechoic chamber. Figure 10 shows the simulated and measured reflection coefficient and the axial ratio of the lens antenna. In addition, the reflection coefficient is lower than −10 dB and the axial ratio is better than 2 dB around 13 GHz. The simulated and measured radiation patterns in the *xoz* plane and *yoz* plane at 13 GHz are illustrated in Fig. 11. It is obvious that the proposed GPGM lens enhances the gain of the patch antenna considerably. Meanwhile, the half power beam width reduces from 80° to 18°. The measured results are in good accordance with the simulation cases.

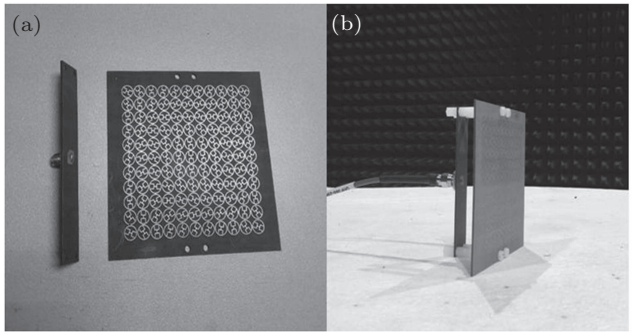


Fig. 9. (a) Prototypes of the proposed GPGM lens antenna and (b) its far-field measured surroundings.

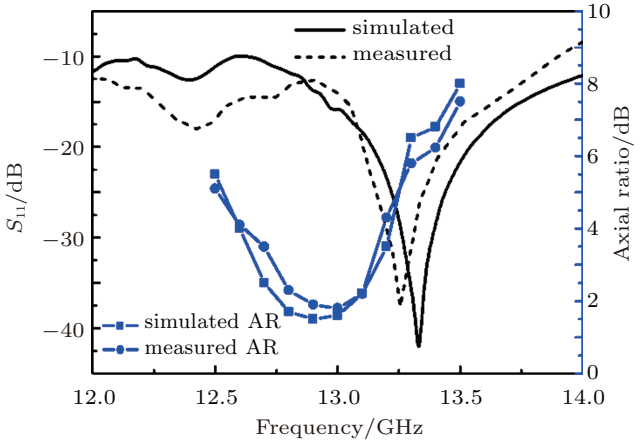


Fig. 10. (color online) Simulated and measured reflection coefficient and axial ratio of the lens antenna.

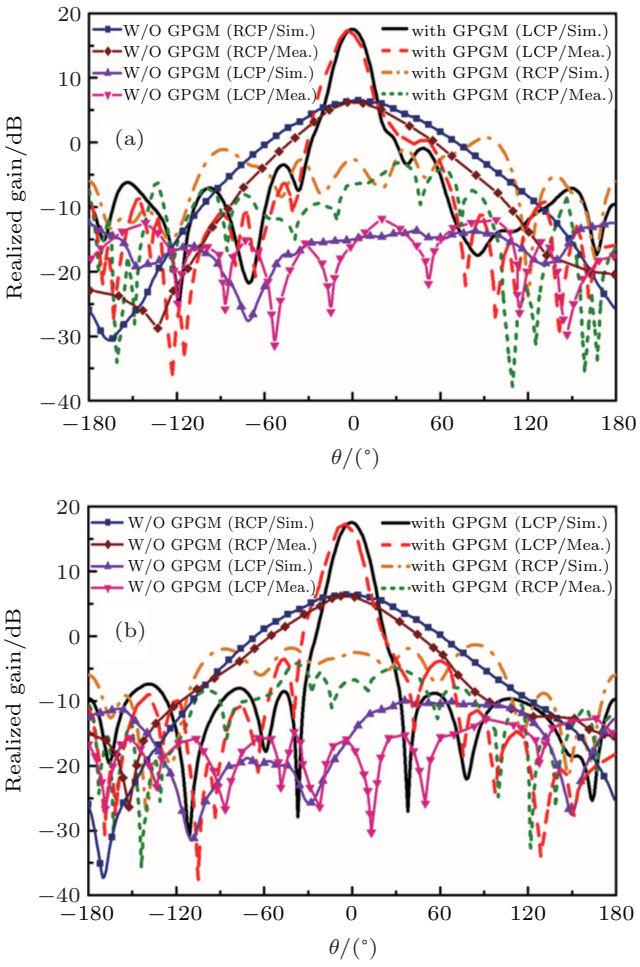


Fig. 11. (color online) Simulated and measured far-field radiation patterns at 13 GHz. (a) *xoz* plane, (b) *yoz* plane.

4. Conclusion and perspectives

In conclusion, a new method to design a CP lens is proposed based on the GPGM. An RCP lens is designed for demonstration of the proposed design method. The lens is single-layered with a thickness of 1.5 mm ($\lambda_0/15$) and a total size of 77 mm×77 mm ($3.3\lambda_0 \times 3.3\lambda_0$). The accuracy phase manipulation and high transmission indicate a perfect focusing effect. For application, an RCP lens antenna working at the Ku band with a F/D of 0.32 is studied numerically and experimentally. The results indicate that the proposed lens antenna achieves a high gain of 17.6 dB at 13 GHz, a good axial ratio of 2 dB, and also a high aperture efficiency of 41%. Remarkably, the planar lens proposed in this paper empowers significant reduction in thickness of the lens, and achieves perfect focusing behavior, low profile, and high transmission efficiency simultaneously, thereby providing a great practical alternative to conventional lenses.

References

[1] Yu N F, Genevet P, Kats M A, Aieta F, Tetienne J P, Capasso F and Gaburro Z 2011 *Science* **334** 333
[2] Cai T, Wang G M, Zhang X F, Wang Y W, Zong B F and Xu H X 2015 *IEEE Trans. Antennas Propag.* **63** 2306
[3] Chen P Y and Alù A 2011 *Phys. Rev. B* **84** 205110
[4] Chen P Y, Argyropoulos C and Alù A 2013 *Phys. Rev. Lett.* **111** 233001
[5] Li Y F, Zhang J Q, Qu S B, Wang J F, Wu X, Xu Z and Zhang A X 2015 *Acta Phys. Sin.* **64** 124102 (in Chinese)
[6] Saeidi C and Weide D 2014 *Appl. Phys. Lett.* **105** 053107
[7] Li X, Xiao S Y, Cai B G, He Q, Cui T J and Zhou L 2012 *Opt. Lett.* **37** 4940
[8] Kuznetsov S A, Astafev M A, Beruete M and Cía M N 2015 *Sci. Rep.* **5** 7738
[9] Cai B G, Li Y B, Jiang W X, Cheng Q and Cui T J 2015 *Opt. Express* **23** 7593
[10] Lee J H, Yoon J W, Jung J, Hong J K, Song S H and Magnusson R 2014 *Appl. Phys. Lett.* **104** 233505
[11] Cai T, Wang G M, Zhang X F, Liang J G, Zhuang Y Q, Liu D and Xu H X 2015 *IEEE Trans. Antennas Propag.* **63** 5629
[12] Cheng J and Mosallaei H 2014 *Opt. Lett.* **39** 2719
[13] Zhu B O, Zhao J M and Feng Y J 2013 *Sci. Rep.* **3** 3059
[14] Li Y F, Zhang J Q, Qu S B, Wang J F, Zheng L, Zhou H, Xu Z and Zhang A X 2015 *Chin. Phys. B* **24** 014202
[15] Yu J B, Ma H, Wang J F, Feng D M, Li Y F and Qu S B 2015 *Acta Phys. Sin.* **64** 178101 (in Chinese)
[16] Phillion R H and Okoniewski M 2011 *IEEE Trans. Antennas Propag.* **59** 1217
[17] Pfeiffer C and Grbic A 2015 *IEEE Trans. Antennas Propag.* **63** 3248
[18] Cai T, Wang G M, Zhang X F and Shi J P 2015 *IEEE Antennas Wirel. Propag. Lett.* **14** 1072